Title

Solution Thermodynamics and Kinetics of Metal Complexation with a Hydroxypyridinone Chelator Designed for Thorium-227 Targeted Alpha Therapy

Journal

Inorganic Chemistry, 57(22)

ISSN

0020-1669

Authors

Deblonde, Gauthier J-P

Lohrey, Trevor D

Booth, Corwin H

et al.

Publication Date

2018-11-19

DOI

10.1021/acs.inorgchem.8b02430

Peer reviewed

Solution Thermodynamics and Kinetics of Metal Complexation with a Hydroxypyridinone Chelator Designed for Thorium-227 Targeted Alpha Therapy

Gauthier J.-P. Deblonde[1], *Trevor D. Lohrey*[1,2], *Corwin H. Booth*[1], *Korey P. Carter*[1], *Bernard F. Parker*[1,2], *Åsmund Larsen*[3], *Roger Smeets*[3], *Olav B. Ryan*[3], *Alan S. Cuthbertson*[*3], *and Rebecca J. Abergel*[*1,4].

[1]Chemical Sciences Division, Lawrence Berkeley National Laboratory, Berkeley, California 94720, USA

[2]Chemistry Department, University of California, Berkeley, California 94720, USA

[3]Department of Thorium Conjugate Research, Bayer AS, 0283 Oslo, Norway

[4]Nuclear Engineering Department, University of California, Berkeley, California 94720, USA

ABSTRACT

The solution chemistry of a chelator developed for ^{227}Th targeted alpha therapy was probed. The compound of interest is an octadentate ligand comprising four *N*-methyl-3-hydroxy-pyridine-2-one metal-binding units, two tertiary amine groups, and one carboxylate arm appended for bioconjugation. The seven pK_a values of the ligand and the stability constants of complexes formed with Th(IV), Hf(IV), Zr(IV), Gd(III), Eu(III), Al(III), and Fe(III) were determined. The ligand exhibits extreme thermodynamic selectivity towards tetravalent metal ions, with a *ca*. 20 orders of magnitude difference between the formation constant of the Th(IV) species formed at physiological pH, namely $[ThL]^{-}$, and that of its Eu(III) analogue. Likewise, log β_{110} values of 41.7 ± 0.3 and 26.9 ± 0.3 (T = 25°C) were measured for $[ThL]^{-}$ and $[Fe^{III}L]^{2-}$, respectively, highlighting the high affinity and selectivity of the ligand for Th ions over potentially competing endogenous metals. Single-crystal structural analysis of the Fe(III) complex revealed a dinuclear 2:2 metal:chelator complex crystallizing in the *P-1* space group. The formation of this dimeric species is likely favored by several intramolecular hydrogen bonds and the protonation state of the chelator in acidic media. L_{III} edge EXAFS data on the Th(IV) complexes of both the ligand and a monoclonal antibody conjugate revealed the expected mononuclear 1:1 metal:chelator coordination environment. This was also confirmed by high resolution mass spectrometry. Finally, kinetic experiments demonstrated that labeling the bioconjugated ligand with Th(IV) could be achieved and

completed after1 hour at room temperature, reinforcing the high suitability of this chelator for ^{227}Th targeted alpha therapy.

KEYWORDS

Thorium, Targeted Alpha Therapy, Bioconjugate, Actinide Chelation

INTRODUCTION

Over the past decade, extensive efforts have been made to develop new therapeutic systems that can take advantage of the tremendous energy released during nuclear decay processes for targeting deleterious cancer cells. Among the different decay modes of radioactive isotopes, the emission of alpha particles is of primary interest within the frame of medical applications. Alpha particles have a high energy and a very short mean free path[1] when compared to beta particles, neutrons, or gamma photons resulting in local deposition of their energy (<100 µm in biological tissue)[2] and affording treatments with lower radiation doses.[3] Although promising, the development of such therapeutics had been hampered until recently by limited access to suitable alpha-emitting isotopes that could fulfill the needs of pharmaceutical markets. Beside transuranic elements (Np, Pu, Am, Cm...), for which short-lived alpha isotopes are abundant in nuclear fuel cycles but are not envisaged for medical applications, several synthetic isotopes have emerged as potential radioactive sources for anti-cancer treatments, as summarized in Table 1. The benefits of using alpha particles as projectiles for neutralizing tumor cells were demonstrated in studies of ^{223}Ra for castration-resistant prostate cancers, eventually leading to the 2013 approval of Xofigo® ($^{223}RaCl_2$) by the U.S. Food and Drug Administration.[4] Nonetheless, Ra being a large divalent cation and an efficient bone-seeker, the inherent lack of strong chelators amenable to safely convey $^{223}Ra^{2+}$ *in vivo* limits its

use in tumor-targeting constructs (such as conjugated antibodies) and hinders its application for broader treatments in oncology.[5]

Commercial production of ^{223}Ra, generated from its parent ^{227}Ac ($t_{1/2}$ = 21.8 y), has also created an opportunity for developing ^{227}Th-based therapy approaches since ^{227}Ac beta-decays to ^{227}Th, which then alpha-decays to ^{223}Ra. In contrast to Ra, Th exhibits the oxidation state +IV in aqueous systems and complexing agents for such a hard metal ion can readily be developed, unleashing the potential for targeted alpha therapy (TAT) strategies based on ^{227}Th bioconjugates. Moreover, as opposed to Ra, the aqueous chemistry of Th(IV) has been extensively studied thanks to the availability of its natural and weakly radioactive isotope ^{232}Th ($t_{1/2}$ = $1.4*10^{10}$ y). Thorium is actually found in several uranium and rare earth element ores and the continental crust contains an average ~10 ppm of ^{232}Th, whereas Ra isotopes are only present at trace levels.[8] The development of Th-based therapeutics could therefore benefit from knowledge of Th(IV) chemistry acquired over past decades as a result of investigations into different nuclear fuel cycles, rare earth and uranium mining,[9] organometallic reactions,[10] and actinide decorporation studies.[11,12]

Table 1. Alpha-particle emitters currently studied for medical applications.

Isotope	Half-life (probability of alpha decay)	Stable oxidation state in aqueous solution	Ionic radius (Å)
^{211}At	7.21 h (41.8 %)	-I	/
^{212}Bi ^{213}Bi	1.01 h (35.9 %) 45.6 min (2 %)	+III	1.17 (CN = 8)[6]
^{223}Ra	11.43 d (100 %)	+II	1.48 (CN = 8)[6]
^{225}Ac	9.95 d (100 %)	+III	1.12 (CN = 6)[6] 1.22 (CN = 9)[7]
^{227}Th	18.68 d (100 %)	+IV	1.05 (CN = 8)[6]

Previous studies on the removal of actinides from the human body have laid an emphasis on siderophore derivatives, a class of compounds that naturally traffics Fe(III) within the blood stream.[13] Siderophore-derived molecules containing hydroxypyridinone (HOPO) groups have shown unprecedented efficacy and selectivity for the *in vitro* and *in vivo* chelation of lanthanides (Ln^{3+}), UO_2^{2+}, Am^{3+}, Zr^{4+}, Sn^{4+}, Ce^{4+}, Pu^{4+}, Bk^{4+}, but also, Th^{4+}.[11,12,14–17] Some of these HOPO-based molecules also exhibit low toxicity compared to classical ligands used for medical applications such as diethylenetriamine pentaacetic acid (DTPA), tetra-azacyclododecane-1,4,7,10-tetraacetic acid (DOTA), or ethylenediamine tetraacetic acid (EDTA).[18] For instance, a bioconjugate of the synthetic chelator 3,4,3-LI(1,2-HOPO), based on 1-hydroxy-pyridine-2-one groups, was recently shown to sequester Zr(IV) *in vivo*, a meaningful result for the development of ^{89}Zr positron emission tomography (Fig. 1).[19] *N*-methyl-3-

hydroxy-pyridine-2-one (Me-3,2-HOPO) analogues, such as TREN-Me-3,2-HOPO (Fig. 1), have also been extensively studied for their ability to complex Gd(III) and subsequent use as magnetic resonance imaging contrast agents.[20] The octadentate Me-3,2-HOPO derivative shown in Figure 1, **L_1**, was developed specifically for ^{227}Th TAT.[21–23] **L_1** displays four bidentate Me-3,2-HOPO binding units and a carboxylic arm that can be used for bioconjugation to larger molecules, such as monoclonal antibodies, via amide coupling.

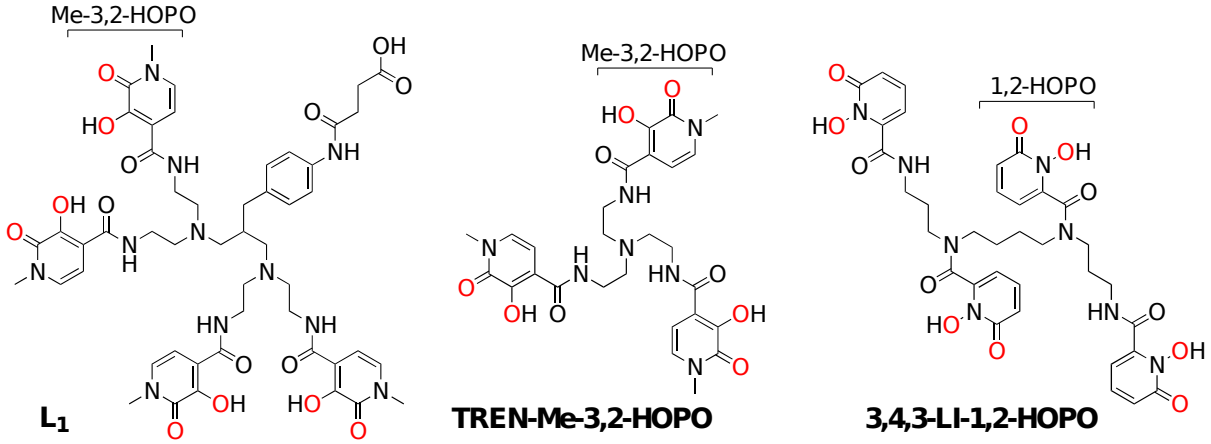

Figure 1. Structures of the octadentate hydroxypyridinone derivative currently investigated for ^{227}Th TAT (**L_1**, left), the hexadentate TREN-Me-3,2-HOPO developed for Gd(III) complexation (center), and the octadentate 3,4,3-LI(1,2-HOPO) currently investigated for ^{89}Zr PET imaging (right). Metal-binding oxygen donors are highlighted in red.

In this work, the solution thermodynamics of **L_1** were investigated. The pKa's of the ligand and the stability constants of its complexes formed with Th(IV), Hf(IV), Zr(IV), Gd(III), Eu(III), Al(III), and Fe(III) were determined, demonstrating the high affinity and selectivity of **L_1** for tetravalent Th ions. Additionally, single crystals of the Fe(III) complex were obtained and their solid-state structure determined. Extended X-Ray Absorption Fine Structure (EXAFS) spectra were collected for the Th(IV)

complexes of **L_1** and of its monoclonal antibody (epratuzumab, abbreviated mAb hereafter) derivative, showing essentially identical metal coordination environment upon bioconjugation. All the results presented herein confirm the unparalleled suitability of **L_1** as a chelator for use in ^{227}Th TAT.

METHODS

Caution! *^{232}Th is an alpha-emitting radionuclide with a half-life of 1.4 × 10^{10} years that should only be manipulated in specifically designated facilities and in compliance with appropriate safety controls.*

General

The purified salt of **L_1** (acidic form) was synthesized by Bayer AS Thorium Conjugate Research (Norway) according to previously published procedures.[23] The salt was stored at -10°C before and after each stock solution preparation. Stock solutions (*ca*. 3-5 mM) were prepared by direct dissolution of the ligand in DMSO and stored at -10°C in between experiments. Stock solutions of the epratuzumab (mAb) conjugate of **L_1** (2.5 mg/mL) in biological buffer (70 mM NaCl, 30 mM citrate, 2 mM EDTA, pH 5.5) were prepared as described previously[21] and stored at -18°C in between experiments. Citric acid (>99.9998%, Sigma-Aldrich), KCl (>99.9995%, Sigma-Aldrich), acetic acid (>99%, Sigma-Aldrich), CHES (>99%, Sigma-Aldrich), HEPES (99%, Sigma-Aldrich), potassium hydrogen phthalate (99.95%, Sigma-Aldrich), $AlCl_3$•$6H_2O$ (99.9995%, Beantown Chemical), $FeCl_3$·$6H_2O$ (>99.95 %, VWR), $ZrCl_4$ (99.99%, Sigma-Aldrich),

$HfCl_4$ (VWR, 99.5%), $GdCl_3 \cdot 6H_2O$ (>99.9%, Sigma-Aldrich), $EuCl_3 \cdot 6H_2O$ (>99.9%, Sigma-Aldrich), and $^{232}ThCl_4 \cdot 8H_2O$ (Baker & Adamson, ACS grade) were purchased from commercial suppliers and were used as received. Metal stock solutions were prepared by direct dissolution of the high purity salts in standard HCl solutions (0.1 M for Eu, Gd, and Fe or 2 M for Th, Hf, and Zr). Hf and Zr salts were weighed under argon atmosphere. Carbonate-free 0.1 M KOH was prepared from Baker *Dilut-It* concentrate and standardized by titrating against 0.1 M potassium hydrogen phthalate. Standard solutions of 0.1 M HCl were purchased form VWR. All solutions were prepared using deionized water purified by a Millipore Milli-Q reverse osmosis cartridge system. Stocks were stored at 8ºC in the dark in between experiments.

The glass electrode (Metrohm - *Micro Combi* - response to $[H^+]$) used for pH measurements was calibrated at 25.0˚C and at an ionic strength of 0.1 M (KCl) before each potentiometric or spectrophotometric titration. Calibration data were analyzed using the program GLEE to refine for E° and slope.[24] The automated titration system was controlled by a 867 pH Module (Metrohm). Two-milliliter Dosino 800 burets (Metrohm) dosed the titrant (0.1 M KOH or 0.1 M HCl) into the thermostated titration vessel (5−90 mL). UV−visible spectra were acquired with an Ocean Optics USB4000-UV−vis spectrophotometer equipped with a TP-300 dip probe (Ocean Optics. Path length of 10 mm), fiber optics and a DH-2000 light source (deuterium and halogen lamps). The automated titration system and the UV-vis spectrophotometer were coordinated by titration system

program, developed in-house. Static UV−visible spectra were measured using a Cary 5G spectrophotometer. All thermodynamic measurements were conducted at 25.0℃, in 0.1 M KCl supporting electrolyte (unless otherwise indicated) under positive argon gas pressure. The entire procedure (sample preparation, titration, and data treatment) was performed in (at least) triplicates to determine each formation constant.

High Resolution Mass Spectrometry (HRMS)

Data were acquired with a Xevo QTOF mass spectrometer (Waters) fitted with an electrospray ionization (ESI) source. Samples were introduced through a reversed phase liquid chromatography column (Poroshell 120 SB-C18, 2.7 µm, 2.1x150 mm, Agilent). The mobile phase was: A = 0.1% trifluoroacetic acid in LCMS water (Fisher) and B = 0.1% trifluoroacetic acid in acetonitrile (Fisher). The gradient was: 5-55% B in 20 min, hold 5 min, back to 5% B in 0.1 min. hold 4.9 min, with a total run time of 30 min. The LC flow was set to 160 µL/min. Ligand **L_1** was dissolved in dimethylacetamide (DMA):water (1:1, v/v) to 5 mg/mL and further diluted to 1 mg/mL with formulation buffer. The formulation buffer composition was 30 mM citrate, 70 mM NaCl, 2 mM EDTA, 0.5 mg/mL 4-aminobenzoic acid, pH = 5.6. An aliquot of **L_1** was added to an equimolar amount of Th or Zr solution and chelation was allowed for 30 minutes at room temperature. The mixture was further diluted to 0.1 mg/mL with formulation buffer prior to analysis.

Incremental Spectrophotometric Titrations

Typically, a 9-mL solution containing 15 µM of the ligand, 15 µM of the metal of interest and the supporting electrolyte was incrementally perturbed by addition of 0.010 mL of 0.1 M KOH followed by a time delay of 60 s. The measurements were done once a stable pH value was reached. Buffering of the solution was ensured by the addition of HEPES, CHES and acetic acid (≤ 3 mM). Between 110 and 190 data points were collected per titration, each data point consisting of a volume increment (0.010 mL), an electrode potential measurement, and an absorbance spectrum (260-750 nm, at intervals of approximately 0.2 nm). Titrations were performed form pH 2 to 12 and at an ionic strength of 0.1 M.

Batch Ligand Competition Titrations Against DTPA

This method was used for the $[Fe^{III}L]^{2-}$ and $[Al^{III}L]^{2-}$ complexes. Typically, 10-12 samples of 3 mL were prepared for each series. Each sample contained 20-30 µM of the ligand and either Fe(III) or Al(III), and from 0 to 100 and 0 to 500 equivalents of DTPA for Fe(III) and Al(III), respectively. Samples were buffered with either 10 or 20 mM HEPES at pH 7.4. The samples were shaken (100 rpm) at 25°C in a shaker-incubator for 10 days to ensure equilibrium. Absorbance spectra were acquired with a SpectraMax Plus 384 spectrophotometer (Molecular Devices). UV-visible spectra were measured in Quartz Suprasil® cuvettes (path length of 10.00 mm) and corrected for buffer absorbance.

Incremental Spectrofluorimetric Titrations

This competition method was used for Eu(III) complexes. Typically, 10-12 samples of 2 mL were prepared per titration. Each sample contained 0.1 µM of Eu(III), 0.1 µM of 3,4,3-LI(1,2-HOPO), and 0 to 30 µM of ligand **L_1**. Samples were buffered with 0.1 M HEPES at pH 7.4. After 24 h of equilibration in a thermostated bath at 25°C, emission spectra were acquired with a HORIBA Jobin Yvon IBH FluoroLog-3 spectrofluorimeter, in steady state mode. Emission (550-725 nm; 350 data points) was monitored perpendicular to the excitation pulse after excitation of the sample at 325 nm. Slits were set at 2.0 nm for the emission and 1.0 nm for the excitation.

Thermodynamic Data Treatment

Spectrophotometric and fluorimetric titration data sets were imported into the refinement program HypSpec[25] and analyzed by nonlinear least-squares refinement. Potentiometric titration data were imported into the refinement program HyperQuad 2008[25] and analyzed by nonlinear least-squares refinement. All equilibrium constants were defined as cumulative formation constants, β_{mlh} according to equation (1), where the metal and ligand are designated as M and L, respectively. For species containing hydroxides, the h value is negative. The list of known stability constants fixed during the refinement processes is given in Table S1.

$$mM+hH+lL \rightleftharpoons \left[M_m H_h L_l\right]; \beta_{mlh}=\frac{\left[M_m H_h L_l\right]}{\left[M\right]^m\left[H\right]^h\left[L\right]^l} \qquad (1)$$

Kinetic Measurements

Kinetics measurements were performed by following UV-visible spectra, using a SpectraMax Plus 384 spectrophotometer (Molecular Devices). Samples of 1.8 mL were prepared in Quartz Suprasil® cuvettes and all experiments were performed at 22°C. Samples were buffered in 70 mM NaCl, 30 mM citrate, pH 5.5, with or without 2 mM of EDTA. All UV-visible spectra were referenced to the corresponding buffer. The free ligand spectrum was recorded at first. Due to the acidity of the metal stock solutions (0.1-2.0 M HCl), an aliquot of KOH corresponding to the amount of HCl induced by the addition of the metal stock was added to the ligand solution prior to metal addition. An equivalent of metal (less than 5 µL of metal stock) was then added into the cuvette and the sample was vortexed for three seconds to ensure homogeneous mixing. The cuvette was placed in the spectrophotometer and the absorbance at 350 nm was recorded at regular intervals. Due to the presence of bubbles in the cuvette, generated by the vortex, a dead-time of 30 s was necessary to avoid perturbation of the spectrophotometric measurements. The final UV-visible spectra (*i.e.* at thermodynamic equilibrium) were recorded after 24 to 36 h.

Crystallography

Single crystals of the Fe(III) complex formed with **L_1** were obtained by vapor diffusion of diethyl ether into a 1:1 solution of $FeCl_3$:**L_1** in methanol:toluene:DMSO (50:40:10) with trace amounts of acetonitrile. Crystals formed over five days at room temperature, were suspended in

paratone oil, inspected under a microscope equipped with a polarizing filter, and cut into pieces of appropriate size. A red blade (0.10 x 0.04 x 0.01 mm^3) was selected and mounted onto a 10-micron MiTiGen dual thickness MicroMount™. The mounted crystal was then immediately placed on the goniometer head of the diffractometer and cooled in a 100(2) K stream of dry nitrogen. Data collection was conducted at the Advanced Light Source (ALS) station 11.3.1 of the Lawrence Berkeley National Laboratory (LBNL), using a silicon-monochromated beam of 16 keV (λ = 0.7749 Å) synchrotron radiation. The Bruker APEX3 software package (including SAINT and SADABS) was used throughout data collection and reduction procedures.[26] The structure was determined and refined using SHELXT and SHELXL-2014 in the WinGX software package.[27,28] Some disorder was observed in the lattice chlorine and solvent water molecules surrounding the $FeCl_3$:**L_1** complex, and was modeled satisfactorily via a combination of PART commands and ISOR restraints (for O3W, Cl1A, and Cl2B) with uncertainty values of 0.005. Figures of the finalized structure were generated using Crystal Maker.[29] CCDC 1818963 contains the supplementary crystallographic information; these data can be obtained free of charge from The Cambridge Crystallographic Data Centre. The crystallographic data and structure refinement of the Fe(III) complex of **L_1** are given in Table 2.

Table 2. Crystallographic data and structure refinement for the Fe(III) complex of $\mathbf{L_1}$.

	$[Fe^{III}_2L_2]Cl_4(H_2O)_8(CH_3CN)_2$ (L = $[C_{50}H_{60}N_{11}O_{15}]^-$)
Chemical formula	$C_{104}H_{142}Cl_4Fe_2N_{24}O_{38}$
Formula weight	2589.91
Color, habit	Red, blade
Temperature (K)	100(2)
Crystal system	Triclinic
Space group	P-1
a (Å)	13.031(6)
b (Å)	15.282(8)
c (Å)	16.629(7)
α (°)	63.453(5)
β (°)	78.055(11)
γ (°)	85.821(6)
V (Å^3)	2897.5
Z	1
Density (Mg m^{-3})	1.484
F(000)	1358
Radiation Type	Synchrotron
μ (mm^{-1})	0.525
Crystal size (mm^3)	0.10 x 0.04 x 0.01
Meas. Refl.	25572
Indep. Refl.	10633
R(int)	0.0341
Final R indices [I > 2σ(I)]	R1 = 0.0815, wR2 = 0.2383
Goodness-of-fit	1.036
$\Delta\rho_{max}$, $\Delta\rho_{min}$ (e Å^{-3})	1.323, -0.997

EXAFS Data Collection

A sample containing 2.0 mM of ^{232}Th(IV) and 1.2 equivalents of the ligand was prepared in biological buffer (70 mM NaCl, 30 mM citrate, 2 mM EDTA, pH 5.5). The sample also contained 30% of DMF to increase the solubility of the complex. Another sample containing the mAb-bioconjugate was assembled as follows: 8 mL of mAb-bioconjugate solution (16.7 µM) in the same buffer were mixed with 0.83 equivalent of $ThCl_4$ and shaken for 60 min at room temperature. The sample was then concentrated 80 times using a VivaSpin® size exclusion filter (cut-off at 5 kDa). EXAFS analysis necessitated 95-µL aliquots of each sample. The mass of ^{232}Th per sample was 46 µg (with ligand) and 25 µg (with mAb-bioconjugate). Both solution samples were loaded into triply contained aluminum holders with Kapton windows within 3 days of data collection, performed at the Stanford Synchrotron Radiation Lightsource (SSRL) - beamline 11-2. A half-tuned Si(220) (ϕ=0°) was used and these Th L_{III}-edge measurements (~16300 eV) were performed using a 100-element Ge detector. A dead time correction was applied. 10 scans (nearly 5 h) of each sample were obtained.

EXAFS Data Treatment

Data were reduced and analyzed using standard described procedures.[30,31] Specifically, the atomic background μ_0 was determined by fitting a constrained 6th-order Chebychev polynomial through the data up to k = 13.8 Å^{-1}. Both data sets were fitted in r-space between 1.5 and 3.7 Å using a transform range between 2.5 and 13.5 Å^{-1}, and narrowed with a 0.3 Å^{-1}-wide Gaussian filter. Back-scattering phases and amplitudes were

calculated using FEFF 10.0.1[32] on the Th(PR-Me-3,2-HOPO) structure reported by Xu et al.[33] While the fit model includes three scattering shells, only the nearest-neighbor Th-O shell fits are well determined. Data errors were determined from the standard deviation of the mean of the 10 scans and parameter errors were determined using a profiling method.[34] Each fit has 8.4 degrees of freedom.[35]

RESULTS AND DISCUSSION

Ligand Protonation

Prior to studying the complexation of metal cations by the investigated ligand **L_1**, acidity constants for the chelator itself were determined. The ligand can be involved in seven acid-base couples since it contains one carboxylic acid, two tertiary amine groups and four Me-3,2-HOPO units. The protonation constants of the ligand were first determined by potentiometry and then confirmed by incremental spectrophotometric titrations (Fig. 2 and S1). The pKa values extrapolated from both techniques are in excellent agreement (Fig. S2). The seven acidity constants span values from 2.9 to 9.6, which covers a broader acidity range compared to other Me-3,2-HOPO chelators with lower denticity, such as the TREN, 5-LI, and 5-LIO derivatives (Table 3). Based on the pKa values reported for these other Me-3,2-HOPO ligands, the highest two pKa values likely correspond to the protonation of the two tertiary amines of **L_1**.

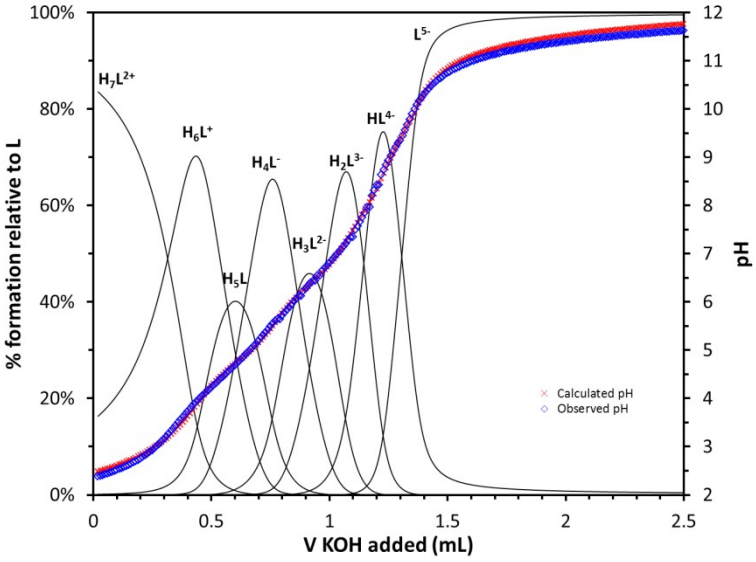

Figure 2. Example of potentiometric titration results obtained for the ligand and corresponding speciation diagram. [$\mathbf{L_1}$] = 1.785 mM. $V_{initial}$ = 9.000 mL. Titrant: 0.1 M KOH. T = 25°C, I = 0.1 M (KCl). pH = 2.4 to 11.7 (275 data points). Results fitted with HyperQuad 2008 (blue diamonds: experimental points; red crosses: model).[25]

Table 3. Protonation constants for $\mathbf{L_1}$ and selected Me-3,2-HOPO ligands.

Ligand	Couple	pKa
$\mathbf{L_1}$	H_7L^{2+}/H_6L^+	2.93 (0.35)[a]
	H_6L^+/H_5L	4.39 (0.08)[a]
	H_5L/H_4L^-	4.73 (0.34)[a]
	H_4L^-/H_3L^{2-}	5.97 (0.14)[a]
	H_3L^{2-}/H_2L^{3-}	6.90 (0.05)[a]
	H_2L^{3-}/HL^{4-}	7.74 (0.06)[a]
	HL^{4-}/L^{5-}	9.58 (0.16)[b]
TREN-Me-3,2-HOPO[36]	H_4L^+/H_3L H_3L/H_2L^- H_2L^-/HL^{2-} HL^{2-}/L^{3-}	4.96 (0.01) 5.80 (0.03) 6.95 (0.03) 8.20 (0.05)
5-LIO(Me-3,2-HOPO)[37]	H_2L/HL^- HL^-/L^{2-}	5.91 (0.01) 7.14 (0.03)
5-LI(Me-3,2-HOPO)[37]	H_2L/HL^- HL^-/L^{2-}	5.94 (0.01) 6.86 (0.03)

[a]Average between potentiometric and spectrophotometric measurements.
[b]Value from potentiometric titrations.

Complexation of Trivalent and Tetravalent Metal Ions

In order to investigate the suitability of bioconjugates based on **L_1** for ^{227}Th TAT, the solution thermodynamics of the unconjugated chelator were first probed. As observed for other HOPO ligands, the four Me-3,2-HOPO groups of **L_1** absorb in the UV-visible region and are sensitive to metal chelation. This feature can be leveraged to characterize the affinity of the chelator for various metal ions, even those that lack convenient spectroscopic properties such as Th(IV). The uptake of Th(IV) ions was first confirmed at pH 7.4 and 5.5 (Fig. S3). At physiological pH, the addition of one equivalent of Th(IV) yields a blue shift from 345 to 340 nm and an increase in the extinction coefficient due to the deprotonation of the Me-3,2-HOPO moieties induced by metal complexation. Formation of a 1:1 complex between Th(IV) and **L_1**, as well as Zr(IV) and **L_1**, was then confirmed by HRMS (Fig. S4). Both complexes were observed as protonated molecules, at respective *m/z* values of 1284.5 and 1142.3, in accordance with the isotopic pattern and elemental composition (Th(IV)-**L_1** = $C_{50}H_{57}N_{11}O_{15}Th$ and Zr(IV)-**L_1** = $C_{50}H_{57}N_{11}O_{15}Zr$), as shown in Figure S4. Based on previous reports on the chelation of tetravalent metal ions with Me-3,2-HOPO derivatives,[11,33] the Th(IV) complexes were expected to be highly stable (log β_{MHL} > 35). Consequently, the formation constant of such strong complexes cannot be measured by direct addition of the ligand to a metal ion solution as complexes would form immediately, even at low pH, and their determination warrants the use of competition titrations. In the presence of a large excess of a competing ligand (here DTPA), the $[ThDTPA]^-$ and [ThHDTPA] complexes form at low pH and ligand exchange occurs upon addition of a base so that Th(IV)-**L_1** complexes are

progressively formed. This technique was previously proven suitable for the study of extraordinarily stable complexes.[38] DTPA was chosen as a competing ligand for its relatively strong affinity towards Th(IV) ions, its silent UV-visible absorbance features and well-characterized solution thermodynamics. Incremental spectrophotometric titrations in the presence of DTPA between pH 2 and 12 confirmed Th(IV) chelation by **L_1** and corresponding UV-visible variations were modeled by the formation of three different species (Fig. 3).

A proton-independent stability constant, log β_{110}, of 41.7 ± 0.3 was determined for the Th complex of **L_1** (Table 4), corresponding to an extremely stable complex compared to those formed with endogenous molecules such as citrates, carbonates, and transferrin.[39] **L_1** is only bested by other synthetic octadentate siderophores such as 3,4,3-LI(1,2-HOPO) or some terephthalamide macrocycles.[12,38] Speciation simulations show that **L_1** is amenable to totally sequester Th(IV) ions at physiological pH even in the presence of more than 10^9 equivalents of citrate ions or EDTA, or 10^7 equivalents of DTPA. Similar experiments with Zr(IV) and Hf(IV) yielded complex formation constants of 44.7 ± 0.1 and 44.8 ± 0.3, respectively (Fig. S5). The higher affinity observed for Zr and Hf compared to Th was expected, owing to the smaller ionic radius of the group IV metal ions compared to Th(IV) and based on results from other HOPO systems.[13,33,37] Even if Zr and Hf ions are not natural competitors for a ^{227}Th-based drug, isotopes of these two elements can potentially be present during the ^{227}Th production process and subsequent radiolabeling step. Due to the high

specific activity of ^{227}Th (1,100 TBq/g), the actual concentration used for alpha therapy injections is typically in the nanomolar or sub-nanomolar range[21] and as a consequence, care must be taken to minimize contamination from trace metal impurities. As an excess of chelator is always present during the radiolabeling step, high levels of incorporation of ^{227}Th are maintained, however the high formation constants determined for Zr(IV) and Hf(IV) ensure that even trace amounts of these elements would also be chelated by **L_1**.

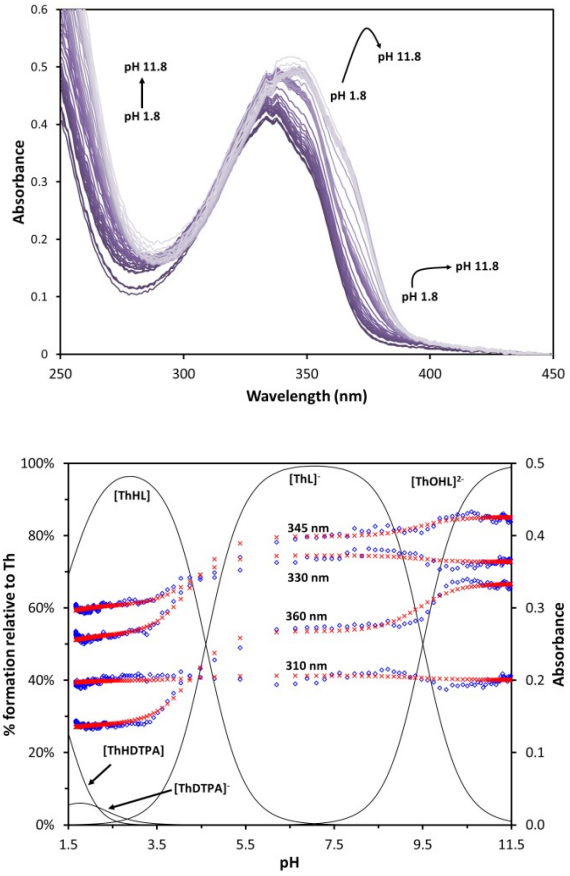

Figure 3. Top panel: Experimental UV-visible spectra from a spectrophotometric titration of the Th(IV) complex (15 µM ligand, 15 µM Th(IV), 1 mM DTPA, 1 mM CHES, 1 mM HEPES, 1 mM MES, 35 mM HCl, 65 mM KCl, I = 0.1 M, T = 25°C); 220 spectra were measured between pH 1.8 and 11.8 and corrected for dilution; data abridged for clarity. Bottom panel: Corresponding speciation diagram and absorbance at 310, 330, 345, and 360 nm at varying pH (blue diamonds: experimental points. red

crosses: values calculated using *HypSpec*). Similar absorbance variations were observed for the corresponding Hf(IV) and Zr(IV) systems (Fig. S5).

Table 4. Stability constants of Th, Hf, Zr, Gd, Eu, Fe, and Al complexes formed with $\mathbf{L_1}$.[a]

	Species	log β_{MHL} for L_1
Th(IV)	$[ThHL]$	45.95 (0.37)[b]
	$[ThL]^-$	41.72 (0.30)[b]
	$[ThH_{-1}L]^{2-}$	32.39 (0.35)[b]
Hf(IV)	$[HfHL]$	50.65 (0.18)[b]
	$[HfL]^-$	44.77 (0.31)[b]
	$[HfH_{-1}L]^{2-}$	35.59 (0.72)[b]
Zr(IV)	$[ZrHL]$	50.81 (0.09)[b]
	$[ZrL]^-$	44.70 (0.14)[b]
	$[ZrH_{-1}L]^{2-}$	33.27 (0.80)[b]
Gd(III)	$[GdHL]^-$	26.14 (0.40)[c]
	$[GdL]^{2-}$	21.08 (0.06)[c]
	$[GdH_{-1}L]^{3-}$	10.4 (0.50)[c]
Eu(III)	$[EuHL]^-$	26.04 (0.04)[c]
	$[EuL]^{2-}$	21.09 (0.02)[c] 21.06 (0.01)[d]
	$[EuH_{-1}L]^{3-}$	10.4 (0.50)[c]
Fe(III)	$[FeHL]^-$	31.2 (0.4)[e]
	$[FeL]^{2-}$	26.9 (0.3)[e]
Al(III)	$[AlL]^{2-}$	20.7 (0.4)[e]

[a]Values obtained at T = 25°C and I = 0.1 M (KCl); standard deviations obtained from three or more measurements are given in parenthesis.
[b]Incremental spectrophotometric measurements in the presence of DTPA.
[c]Incremental spectrophotometric measurements.
[d]Fluorimetric batch titrations.
[e]Ligand competition spectrophotometric batch titrations.

Taking advantage of the absorbance properties of the Me-3,2-HOPO moieties and their sensitivity to metal chelation, the uptake of Zr(IV) and

Th(IV) by a **L_1**-mAb conjugate was followed by monitoring the absorbance band of the conjugated chelator between 280 and 400 nm. The protein itself absorbs at lower wavelengths and does not completely overlap with the absorbance of the HOPO units (Fig. 4). Upon addition of one equivalent of $ZrCl_4$ or $ThCl_4$ to the bioconjugate in a typical pharmaceutical formulation (70 mM NaCl, 30 mM citrate, 2 mM EDTA, pH 5.5), the absorbance band of the HOPO units at around 350 nm becomes more intense, similar to what is observed for the small chelator itself (Fig. 4 and S3).

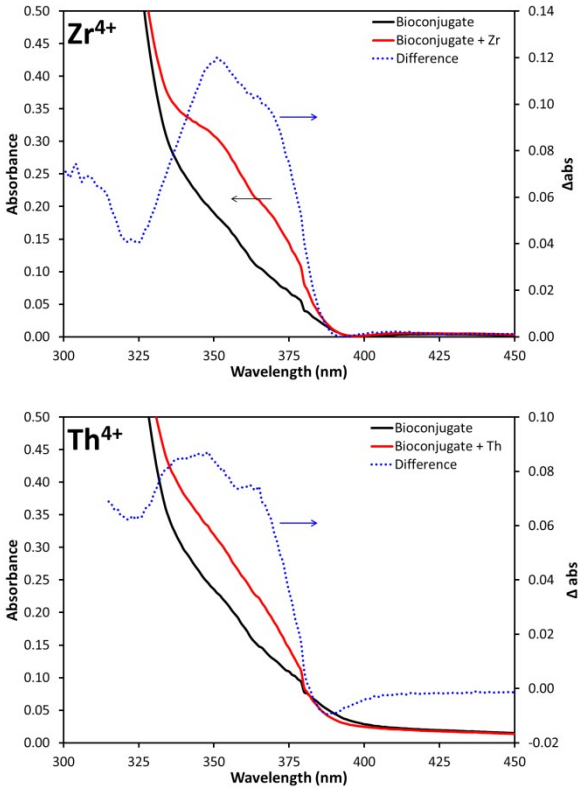

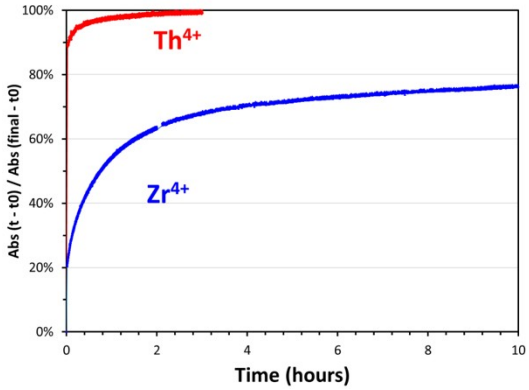

Figure 4. UV-vis spectra of the **L_1**-mAb conjugate without (black) and with 1 equivalent of tetravalent metal (red) Zr(IV) (top) or Th(IV) (center) at equilibrium; the difference between each of the two spectra is shown as blue dotted curve. Bottom panel: Relative changes in absorbance observed at 350 nm upon addition of 1 equivalent of $ThCl_4$ (red) or $ZrCl_4$ (blue) to the **L_1**-mAb. [**L_1**-mAb] = 2.5 mg/L ~ 16.7 µM. [Zr] = [Th] = 0 or 16.7 µM, 70 mM NaCl, 30 mM citric acid, 2 mM EDTA, pH = 5.5, T = 22°C, 10-mm path length.

This clearly indicates that metal ions are bound to the Me-3,2-HOPO groups of the ligand, with no interfering non-specific binding to the macromolecule. Absorbance monitoring at 350 nm over time shows that radiolabeling with Th(IV) is complete after about one hour at room temperature (Fig. 4, bottom panel). The uptake of Zr(IV) by the same **L_1**-mAb conjugate was found much slower (more than 24 h at 22°C) than in the case of Th(IV), a difference likely due to the presence of EDTA in the formulation, which binds Zr(IV) first and then slowly exchanges it with the bioconjugate. Experiments with the non-conjugated ligand, in the absence or presence of EDTA, revealed that EDTA readily slows down the uptake of Zr(IV) by **L_1** (Fig. S6), which could eventually help removing Zr(IV) if present in the process.

The interactions between **L_1** and trivalent Ln cations were also investigated, since Ln fission products can potentially be formed during

the production of ^{227}Th and therefore traces of these 4f-elements may also be present during the radiolabeling procedures. Incremental spectrophotometric titrations were used to determine the stability constants of the Eu(III) and Gd(III) complexes, and variations in the UV-visible absorbance at varying pH were modeled by the formation of three different complexes between pH 3.5 and 12 (Fig. 5, top panel). In order to confirm the reliability of the speciation model, the formation constant of the unprotonated Eu(III) complex formed at near-neutral pH, $[EuL]^{2-}$, was confirmed by spectrofluorimetry. Using the luminescent properties of the Eu(III) complex of 3,4,3-LI(1,2-HOPO), a ligand known for sensitizing Eu(III) at physiological pH,[14,40] and of the silent properties of the Eu(III) complex of **L_1**, the stability constant of the **L_1** complex could be assessed. Addition of 10 to 100 equivalents of **L_1** to a 1:1 solution of Eu(III):3,4,3-LI(1,2-HOPO) progressively turns off the Eu(III) emission due to the formation of the silent **L_1** complex (Fig. 5, bottom panel). Refinement of the titration data for the Eu(III)-**L_1** and Gd(III)-**L_1** systems yielded stability constants of $10^{21.1}$ for both $[EuL]^{2-}$ and $[GdL]^{2-}$, identical within the experimental uncertainty (Table 4). Octadentate HOPO-based molecules usually exhibit a high selectivity toward tetravalent metals ions at the expense of the trivalent ions.[12,15] The difference in stability constants between the Th(IV) and Eu(III) complexes is extremely high ($\Delta\log \beta_{110} = 19.9$) and highlights the suitability of **L_1** for ^{227}Th complexation.

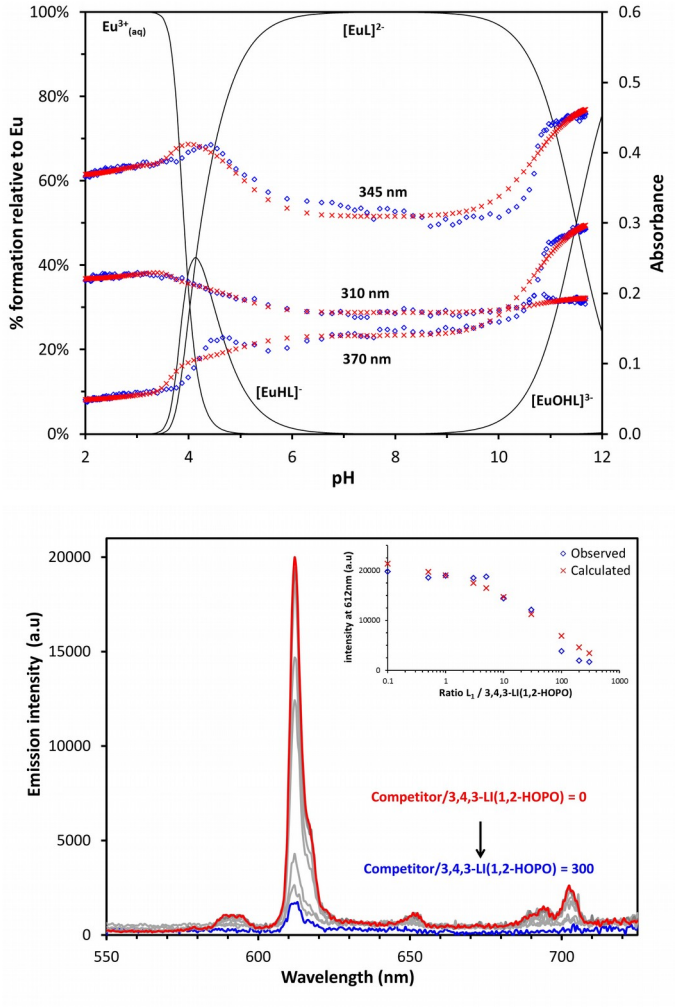

Figure 5. Top panel: Speciation diagram and absorbance variations at 310, 345, and 370 nm as a function of pH observed for the Eu(III)-**L_1** system (blue diamonds are experimental points and red crosses are calculated values). Full spectra were acquired between 250 and 450 nm but only three wavelengths are shown for clarity. Starting conditions: 15 µM **L_1**, 15 µM Eu(III), 3 mM CHES, 3 mM HEPES, 3 mM MES, 15 mM HCl and 85 mM KCl (I = 0.1 M), T = 25°C; 190 spectra were acquired between pH 1.8 and 11.7. Bottom panel: Example of fluorimetric competition titration between **L_1** and 3,4,3-LI(1,2-HOPO) toward Eu(III) binding. [Eu] = 0.1 µM, [3,4,3-LI(1,2-HOPO)] = 0.1 µM, [**L_1**] = 0 to 30 µM, I = 0.1 M (HEPES, pH 7.4), T = 25°C. $\lambda_{excitation}$ = 325 nm. Inset: Emission intensity at 612 nm as a function of the **L_1**:3,4,3-LI(1,2-HOPO) ratio.

Additionally, the binding of **L_1** to Fe(III) was probed in order to evaluate the propensity of the chelator to complex endogenous metals. Addition of one equivalent of Fe(III) to **L_1** immediately yields a light red solution with a large absorbance band between 400 and 700 nm and two local maxima at

433 and 541 nm. Similar ligand-to-metal charge transfer bands have been reported for two other Me-3,2-HOPO derivatives.[41,42] Initial attempts to assess the stability constant of the Fe(III) complex by incremental spectrophotometric titration in the presence of DTPA failed due to the very slow ligand exchange between DTPA and **L_1**. Without the presence of a competing ligand, Fe(III) was already bound to **L_1** even at pH 1 (Fig. S7) and the incremental spectrophotometric titrations revealed only one acid-base equilibrium for the Fe(III) system around pH 4. The Fe(III) complex formation constant was measured by ligand competition batch titrations at fixed pH. The exchange between DTPA and **L_1** at pH 7.4 was complete after 7 days at 25°C and more than 10 equivalents of DTPA were necessary to displace Fe(III) from **L_1** (Fig. 6). Refinement of the titration data yielded stability constants of 31.2 and 26.9 for $[FeHL]^-$ and $[FeL]^{2-}$, respectively. These values are in the same range as those of the Fe(III) complexes formed with the hexadentate ligand TREN-Me-3,2-HOPO.[41] Fe(III) complexes of **L_1** are also less stable than their Th(IV) counterparts by several orders of magnitude (Table 4) and the release, *in vivo*, of Th by transmetallation with Fe is unlikely to occur.

Finally, **L_1** binding to Al(III) was explored as Al was found to be a potential trace impurity in formulated bioconjugate solutions. Initial attempts to determine the stability constant of the Al(III) complex via metal competition batch titrations with Fe(III) were unsuccessful as Al(III) was unable to displace Fe(III), even when present in large excess (1000 equivalents). Eu(III) was then tested in place of Fe(III) for metal

competition titrations, yet this was also unsuccessful as metal exchange between Eu(III) and Al(III) was not straightforward, with mixed metal-ligand species likely forming. As a result, the Al(III) complex formation constant was then measured by ligand competition batch titrations at fixed pH, similar to the procedure described above for Fe(III). The exchange between DTPA and **L_1** at pH 7.4 was found to be complete after 7 days at 25°C and more than 50 equivalents of DTPA were necessary to displace Al(III) from **L_1** (Fig. S8). Refinement of the titration data yielded a stability constant of 20.7 for $[AlL]^{2-}$ indicating the Al(III) complexes of **L_1** are less stable than their Fe(III) counterparts by several orders of magnitude (Table 4), which is consistent with previous studies comparing formation constants of Fe(III) and Al(III) with HOPO complexes.[43]

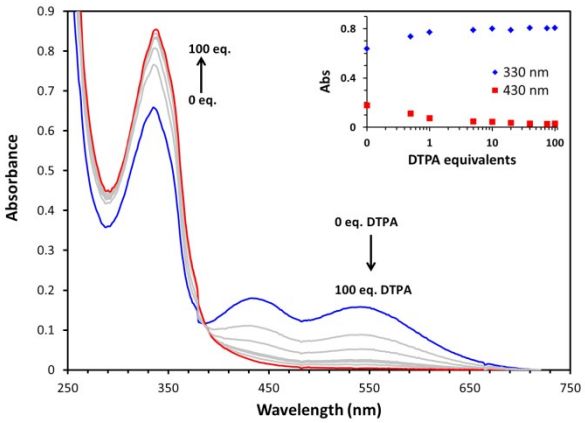

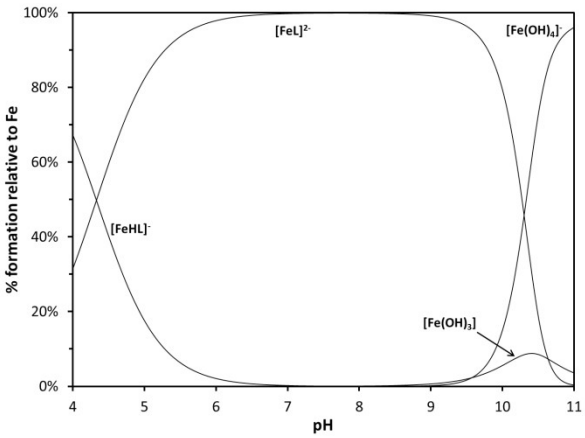

Figure 6. Top panel: Spectrophotometric competition batch titration of $[FeL]^{2-}$ using DTPA as competing ligand. [Fe] = [**L₁**] = 30 μM, [DTPA] = 0 to 100 equivalents, pH = 7.4 (10 mM HEPES), T = 25°C, I = 0.1 M (KCl), 10-mm path length. Inset: change observed at 430 (squares) and 330 nm (diamond) as a function of the DTPA:**L₁** ratio. Bottom panel: speciation diagram of the Fe(III)-**L₁** system.

Structural characterization

Several attempts were performed in order to obtain crystal structures of the Th(IV), Zr(IV), Hf(IV), or Eu(III) complexes of **L₁**. Unfortunately, crystallization assays were unsuccessful with these elements, and the only crystalline material obtained was with Fe(III). X-ray quality single crystals were obtained by vapor diffusion of diethyl ether into a 1:1 solution of $FeCl_3$ and **L₁** in methanol:toluene:DMSO with trace amounts of acetonitrile. The crystal structure revealed a centrosymmetric dinuclear 2:2 complex with two Fe(III) centers and two complete ligands (Fig. 7). The Fe(III) cations are each hexacoordinated by two Me-3,2-HOPO units from one ligand molecule and one Me-3,2-HOPO unit from a second molecule, leaving one unchelated Me-3,2-HOPO unit per molecule. The average Fe-O distance is 2.009(5) Å, with the shortest bond at 1.987(3) Å and the longest at 2.039(3) Å, which is within the range of what was previously reported for other Fe(III) complexes containing three Me-3,2-HOPO units.[41] The two secondary amines of the chelator, as well as its unchelated Me-3,2-HOPO unit and carboxylic acid-appended arm, were protonated, a likely result of HCl from the Fe(III) stock solution in the crystallization solution. As a result, the whole Fe(III) complex is positively charged and charge-balanced by chloride ions. The observed conformation of **L₁** in the

solid state appears to be driven by several hydrogen bonds, including both intramolecular interactions within Me-3,2-HOPO moieties as well as intermolecular interactions between **L_1** units and outer sphere water molecules and chloride anions. Whereas intramolecular hydrogen bonding interactions only occur between acceptors and donors within the same **L_1** molecule, (with most serving to enforce planarity between the Me-3,2-HOPO units and their corresponding amide linking moieties) it is apparent that the protonated tertiary amines each act as hydrogen bond donors. Therefore, the conformation and nuclearity of the Fe(III) complex with **L_1** may change significantly at higher pH, depending on the protonation state of the tertiary amines.

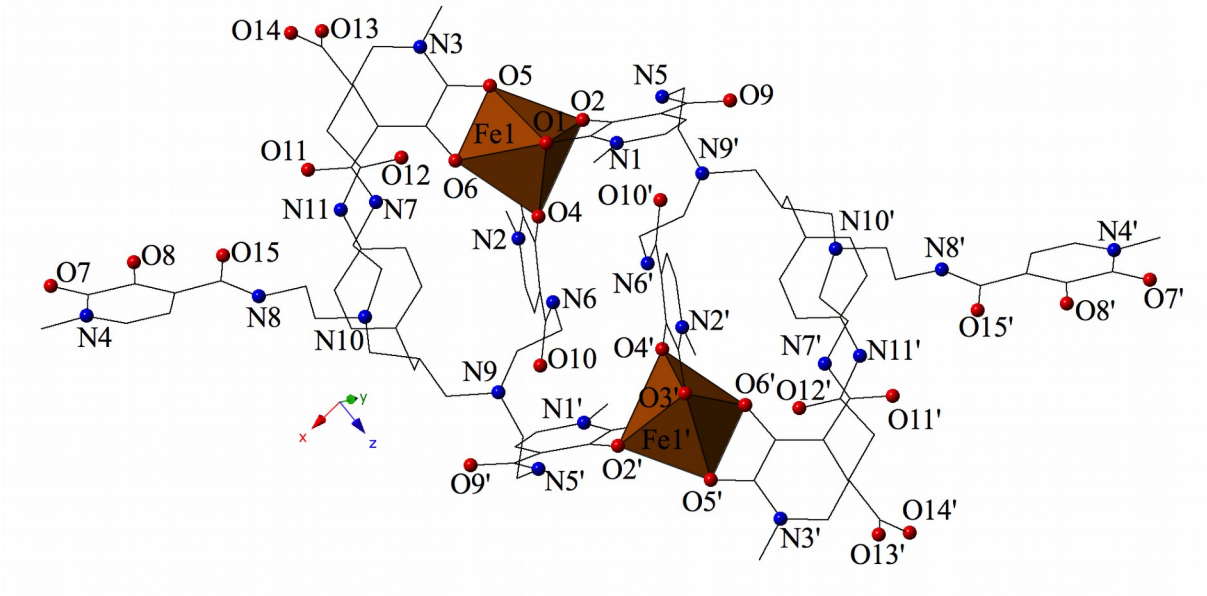

Figure 7. Polyhedral representation of the Fe(III) complex of **L_1**. Orange polyhedral are Fe(III) centers, whereas spheres represent oxygen atoms (red) and nitrogen atoms (blue). Hydrogen atoms, chloride ions, and solvent molecules are omitted for clarity.

Since single crystals of the Th(IV) complex could not be obtained, structural information on the Th system was gained via extended X-ray

absorbance fine structure (EXAFS) spectroscopy. EXAFS spectra at the Th L_{III} edge were collected for both **L_1** and its mAb bioconjugate complexes in a representative pharmaceutical formulation. The EXAFS spectra of both samples were found to be very similar (Fig. 8). The structural fitting results for both the **L_1** complex and that of its mAb conjugate are listed in Table S2. The EXAFS signals are reasonably well described by a fitting model comprising 9.2(9) oxygen atoms at a distance of 2.429(7) in the case of the chelator, and 7.7(5) oxygen atoms at a distance of 2.444(6) in the case of the bioconjugate, assuming a data reduction factor $S_0^2 = 1.0$, as is common for actinide solution systems. The decrease in the number of neighboring oxygen atoms from 9.2(9) to 7.7(5) is thought to be due to the presence of a water molecule in the chelator complex. The Th-O bond distances extrapolated from the EXAFS data are in excellent agreement with those measured from the previously reported crystal structure of $Th(PR\text{-}Me\text{-}3,2\text{-}HOPO)_4$ *i.e.* 2.524(11) for the four Th-O_{oxo} bonds and 2.405(8) for the four Th-$O_{phenolic}$ bonds.[33] The two types of oxygens present in the Me-3,2-HOPO moieties could not be differentiated by EXAFS so the values reported here are an average between the Th-O_{oxo} and Th-$O_{phenolic}$ bonds. The fact that the EXAFS spectra for the chelator and its bioconjugate are very similar highlights that no change in the metal environment occurs when the chelator is conjugated to a macromolecule and provides confirmation that the expected mononuclear 1:1 metal:chelator complexes are maintained upon bioconjugation of **L_1** ligand.

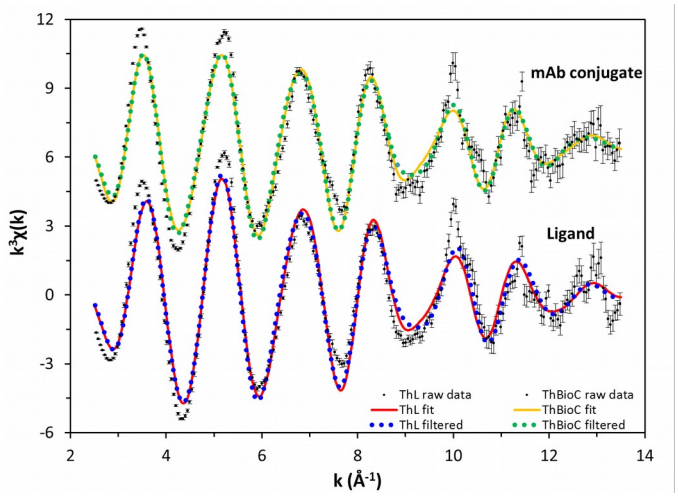

Figure 8. EXAFS data and fit results for aqueous solutions containing the Th(IV) complex of **L_1** (bottom) and that of its mAb conjugate (top). The raw data points reveal error bars estimated by the standard deviation of the mean from 10 traces. The filtered data and fit are back-transformed over the fit range (see ESI for details). The filtered data and fit curves are essentially superimposed. Note that the fit in k-space (solid lines) is properly compared to the filtered data (dotted lines), not the raw data. Ordinates have been shifted for clarity. Corresponding EXAFS data and fit in the r-space are given in Figure S9.

Conclusion

The solution chemistry of **L_1**, a novel chelator currently under development for ^{227}Th targeted alpha therapies, was investigated. This octadentate ligand was found to have a tremendous affinity for tetravalent metal ions such as Th(IV), Zr(IV), Hf(IV), while exhibiting only a moderate affinity for trivalent metals like Eu(III), Fe(III), and Al(III). The very high stability constant of the Th(IV) complex (log β_{ThL} = 41.7) and the charge-dependent selectivity of the chelator ensure that the radioisotope remains sequestered and that no transmetallation with Fe(III) occurs *in vivo*. Uptake experiments with a mAb conjugate of **L_1** revealed that the metal ions are bound to the Me-3,2-HOPO units of the conjugated chelator and fast radiolabeling kinetics were observed. EXAFS spectra on both the

small molecule chelator and the mAb conjugate confirmed that the coordination environment of Th(IV) is not significantly impacted upon bioconjugation. All results confirm the promise of **L_1** as a new chelator for ^{227}Th targeted alpha therapies.

ASSOCIATED CONTENT

Supporting Information. Additional experimental results, including spectrophotometric data, high-resolution mass spectra of Zr(IV) and Th(IV) complexes, EXAFS data and fit parameters. This material is available free of charge via the Internet at http://pubs.acs.org

ACKNOWLEDGMENT

This work was supported by Bayer AS and performed at LBNL, operating under U.S. Department of Energy Contract (DOE) No. DE-AC02-05CH11231 (R.J.A.). EXAFS analysis of Th complexes was supported by DOE's Office of Science, Office of Basic Energy Sciences, Chemical Sciences, Geosciences, and Biosciences Division at LBNL under Contract No. DE-AC02-05CH11231 (C.H.B.) The ALS is supported by the Director, Office of Science, Office of Basic Energy Sciences, of the DOE under Contract No. DE-AC02-05CH11231. Use of the SSRL, SLAC National Accelerator Laboratory, is supported by the DOE, Office of Science, Office of Basic Energy Sciences under Contract No. DE-AC02-76SF00515. We thank Dr. Simon J. Teat of ALS station 11.3.1 for training and oversight of our single crystal X-ray diffraction studies. T.D.L. thanks the DOE Integrated University Program for a graduate research fellowship.

AUTHOR INFORMATION

Corresponding Authors

* abergel@berkeley.edu

* alan.cuthbertson@bayer.com

Notes

The authors declare no competing financial interest.

REFERENCES

(1) Tavernier, S. Interactions of Particles in Matter. In *Experimental Techniques in Nuclear and Particle Physics*; Springer Berlin Heidelberg: Berlin, Heidelberg, 2009; pp 23–53.
(2) Imam, S. K. Advancements in Cancer Therapy with Alpha-Emitters: A Review. *Int. J. Radiat. Oncol. Biol. Phys.* **2001**, *51*, 271–278.
(3) Graf, F.; Fahrer, J.; Maus, S.; Morgenstern, A.; Bruchertseifer, F.; Venkatachalam, S.; Fottner, C.; Weber, M. M.; Huelsenbeck, J.; Schreckenberger, M.; Kaina, B.; Miederer, M. DNA Double Strand Breaks as Predictor of Efficacy of the Alpha-Particle Emitter Ac-225 and the Electron Emitter Lu-177 for Somatostatin Receptor Targeted Radiotherapy. *PLoS ONE* **2014**, *9*, e88239.
(4) Parker, C.; Nilsson, S.; Heinrich, D.; Helle, S. I.; O'Sullivan, J. M.; Fosså, S. D.; Chodacki, A.; Wiechno, P.; Logue, J.; Seke, M.; Widmark, A.; Johannessen, D.C.; Hoskin, P.; Bottomley, D.; James, N.D.; Solberg, A.; Syndikus, I.; Kliment, J.; Wedel, S.; Boehmer, S.; Dall'Oglio, M.; Franzén, L.; Coleman, R.; Vogelzang, N.J.; O'Bryan-Tear, C.G.; Staudacher, K.; Garcia-Vargas, J.; Shan, M.; Bruland, ø. S.; Sartor, O. Alpha Emitter Radium-223 and Survival in Metastatic Prostate Cancer. *N. Engl. J. Med.* **2013**, *369*, 213–223.
(5) Gott, M.; Steinbach, J.; Mamat, C. The Radiochemical and Radiopharmaceutical Applications of Radium. *Open Chem.* **2016**, *14*, 118–129.
(6) Shannon, R. D. Revised Effective Ionic Radii and Systematic Studies of Interatomic Distances in Halides and Chalcogenides. *Acta Crystallogr. A* **1976**, *32*, 751–767.
(7) Lundberg, D.; Persson, I. The Size of Actinoid(III) Ions - Structural Analysis vs. Common Misinterpretations. *Coord. Chem. Rev.* **2016**, *318*, 131–134.
(8) Taylor, S. R. Abundance of Chemical Elements in the Continental Crust: A New Table. *Geochim. Cosmochim. Acta* **1964**, *28*, 1273–1285.
(9) Beltrami, D.; Cote, G.; Mokhtari, H.; Courtaud, B.; Moyer, B. A.; Chagnes, A. Recovery of Uranium from Wet Phosphoric Acid by Solvent Extraction Processes. *Chem. Rev.* **2014**, *114*, 12002–12023.
(10) Garner, M. E.; Parker, B. F.; Hohloch, S.; Bergman, R. G.; Arnold, J. Thorium Metallacycle Facilitates Catalytic Alkyne Hydrophosphination. *J. Am. Chem. Soc.* **2017**, *139*, 12935–12938.
(11) Sturzbecher-Hoehne, M.; Deblonde, G. J.-P.; Abergel, R. J. Solution Thermodynamic Evaluation of Hydroxypyridinonate Chelators 3,4,3-LI(1,2-HOPO) and 5-LIO(Me-3,2-HOPO) for UO_2(VI) and Th(IV) Decorporation. *Radiochim. Acta* **2013**, *101*, 359–366.

(12) Deblonde, G. J.-P.; Sturzbecher-Hoehne, M.; Abergel, R. J. Solution Thermodynamic Stability of Complexes Formed with the Octadentate Hydroxypyridinonate Ligand 3,4,3-LI(1,2-HOPO): A Critical Feature for Efficient Chelation of Lanthanide(IV) and Actinide(IV) Ions. *Inorg. Chem.* **2013**, *52*, 8805–8811.
(13) Gorden, A. E. V.; Xu, J.; Raymond, K. N.; Durbin, P. Rational Design of Sequestering Agents for Plutonium and Other Actinides. *Chem. Rev.* **2003**, *103*, 4207–4282.
(14) Abergel, R. J.; D'Aléo, A.; Ng Pak Leung, C.; Shuh, D. K.; Raymond, K. N. Using the Antenna Effect as a Spectroscopic Tool: Photophysics and Solution Thermodynamics of the Model Luminescent Hydroxypyridonate Complex [Eu(III)(3,4,3-LI(1,2-HOPO))]$^{-}$. *Inorg. Chem.* **2009**, *48*, 10868–10870.
(15) Deblonde, G. J.-P.; Sturzbecher-Hoehne, M.; Rupert, P. B.; An, D. D.; Illy, M.-C.; Ralston, C. Y.; Brabec, J.; de Jong, W. A.; Strong, R. K.; Abergel, R. J. Chelation and Stabilization of Berkelium in Oxidation State +IV. *Nat. Chem.* **2017**, 9, 843-849.
(16) Sturzbecher-Hoehne, M.; Kullgren, B.; Jarvis, E. E.; An, D. D.; Abergel, R. J. Highly Luminescent and Stable Hydroxypyridinonate Complexes: A Step Towards New Curium Decontamination Strategies. *Chem. - Eur. J.* **2014**, *20*, 9962–9968.
(17) Deblonde, G. J.-P.; Lohrey, T. D.; An, D. D.; Abergel, R. J. Toxic Heavy Metal – Pb, Cd, Sn – Complexation by the Octadentate Hydroxypyridinonate Ligand Archetype 3,4,3-LI(1,2-HOPO). *New J. Chem.* **2018**, *42*, 7649–7658.
(18) An, D. D.; Kullgren, B.; Jarvis, E. E.; Abergel, R. J. From Early Prophylaxis to Delayed Treatment: Establishing the Plutonium Decorporation Activity Window of Hydroxypyridinonate Chelating Agents. *Chem. Biol. Interact.* **2017**, *267*, 80–88.
(19) Deri, M. A.; Ponnala, S.; Kozlowski, P.; Burton-Pye, B. P.; Cicek, H. T.; Lewis, J. S.; Francesconi, L. C. P-SCN-Bn-HOPO: A Superior Bifunctional Chelator for ^{89}Zr ImmunoPET. *Bioconjug. Chem.* **2015**, *26*, 2579–2591.
(20) Datta, A.; Raymond, K. N. Gd−Hydroxypyridinone (HOPO)-Based High-Relaxivity Magnetic Resonance Imaging (MRI) Contrast Agents. *Acc. Chem. Res.* **2009**, *42*, 938–947.
(21) Hagemann, U. B.; Wickstroem, K.; Wang, E.; Shea, A. O.; Sponheim, K.; Karlsson, J.; Bjerke, R. M.; Ryan, O. B.; Cuthbertson, A. S. In Vitro and In Vivo Efficacy of a Novel CD33-Targeted Thorium-227 Conjugate for the Treatment of Acute Myeloid Leukemia. *Mol. Cancer Ther.* **2016**, *15*, 2422–2431.
(22) Hagemann, U. B.; Mihaylova, D.; Uran, S. R.; Borrebaek, J.; Grant, D.; Bjerke, R. M.; Karlsson, J.; Cuthbertson, A. S. Targeted Alpha Therapy Using a Novel CD70 Targeted Thorium-227 Conjugate in in Vitro and in Vivo Models of Renal Cell Carcinoma. *Oncotarget* **2017**, *8*, 56311–56326.
(23) Ramdahl, T.; Bonge-Hansen, H. T.; Ryan, O. B.; Larsen, Å.; Herstad, G.; Sandberg, M.; Bjerke, R. M.; Grant, D.; Brevik, E. M.; Cuthbertson,

A. S. An Efficient Chelator for Complexation of Thorium-227. *Bioorg. Med. Chem. Lett.* **2016**, *26*, 4318–4321.
(24) Gans, P.; O'Sullivan, B. GLEE, a New Computer Program for Glass Electrode Calibration. *Talanta* **2000**, *51*, 33–37.
(25) Gans, P.; Sabatini, A.; Vacca, A. Investigation of Equilibria in Solution. Determination of Equilibrium Constants with the HYPERQUAD Suite of Programs. *Talanta* **1996**, *43*, 1739–1753.
(26) Bruker. *SADABS, APEX3, and SAINT*; Bruker AXS: Madison, Wisconsin, USA.
(27) Sheldrick, G. M. A Short History of SHELX. *Acta Crystallogr. A* **2008**, *64*, 112–122.
(28) Farrugia, L. J. WinGX and ORTEP for Windows: An Update. *J. Appl. Crystallogr.* **2012**, *45*, 849–854.
(29) Palmer, D. C. *CrystalMaker*; CrstalMaker Software Ltd.: Begbroke, Oxfordshire, England, **2014**.
(30) Li, G. G.; Bridges, F.; Booth, C. H. X-Ray-Absorption Fine-Structure Standards: A Comparison of Experiment and Theory. *Phys. Rev. B* **1995**, *52*, 6332.
(31) Hayes, T. M.; Boyce, J. B. *Extended X-Ray Absorption Fine-Structure Spectroscopy*; Academic: New York, 1982; Vol. 37.
(32) Rehr, J.; Kas, J.; Vila, F.; Prange, M.; Jorissen. Parameter-Free Calculations of X-Ray Spectra with FEFF9. *Phys. Chem. Chem. Phys.* **2010**, *12*, 5502.
(33) Xu, J.; Whisenhunt, D. W.; Veeck, A. C.; Uhlir, L. C.; Raymond, K. N. Thorium(IV) Complexes of Bidentate Hydroxypyridinonates. *Inorg. Chem.* **2003**, *42*, 2665–2674.
(34) Booth, C. H.; Hu, Y.-J. Confirmation of Standard Error Analysis Techniques Applied to EXAFS Using Simulations. *J. Phys. Conf. Ser.* **2009**, *190*, 012028.
(35) Stern, E. A. Number of Relevant Independent Points in X-Ray-Absorption Fine-Structure Spectra. *Phys. Rev. B* **1993**, *48*, 9825.
(36) Xu, J.; Franklin, S. J.; Whisenhunt Jr, D. W.; Raymond, K. N. Gadolinium Complex of Tris [(3-Hydroxy-1-Methyl-2-Oxo-1, 2-Didehydropyridine-4-Carboxamido) Ethyl]-Amine: A New Class of Gadolinium Magnetic Resonance Relaxation Agents. *J. Am. Chem. Soc.* **1995**, *117*, 7245–7246.
(37) Xu, J.; Radkov, E.; Ziegler, M.; Raymond, K. N. Plutonium(IV) Sequestration: Structural and Thermodynamic Evaluation of the Extraordinarily Stable Cerium(IV) Hydroxypyridinonate Complexes. *Inorg. Chem.* **2000**, *39*, 4156–4164.
(38) Pham, T. A.; Xu, J.; Raymond, K. N. A Macrocyclic Chelator with Unprecedented Th^{4+} Affinity. *J. Am. Chem. Soc.* **2014**, *136*, 9106–9115.
(39) Martell, A. E.; Smith, R. M.; Motekaitis, R. J. NIST Standard Reference Database 46. National Institute of Standards and Technology: Gaithersburg, MD, USA.
(40) Sturzbecher-Hoehne, M.; Ng Pak Leung, C.; D'Aléo, A.; Kullgren, B.; Prigent, A.-L.; Shuh, D. K.; Raymond, K. N.; Abergel, R. J. 3,4,3-LI(1,2-HOPO): In Vitro Formation of Highly Stable Lanthanide Complexes

Translates into Efficacious in Vivo Europium Decorporation. *Dalton Trans.* **2011**, *40*, 8340.
(41) Xu, J.; O'Sulliva, B.; Raymond, K. N. Hexadentate Hydroxypyridonate Iron Chelators Based on TREN-Me-3, 2-HOPO: Variation of Cap Size1. *Inorg. Chem.* **2002**, *41*, 6731–6742.
(42) Scarrow, R. C.; Riley, P. E.; Abu-Dari, K.; White, D. L.; Raymond, K. N. Ferric Ion Sequestering Agents. 13. Synthesis, Structures, and Thermodynamics of Complexation of Cobalt (III) and Iron (III) Tris Complexes of Several Chelating Hydroxypyridinones. *Inorg. Chem.* **1985**, *24*, 954–967.
(43) Santos, M. A.; Gil, M.; Marques, S.; Gano, L.; Cantinho, G.; Chaves, S. N-Carboxyalkyl Derivatives of 3-Hydroxy-4-Pyridinones: Synthesis, Complexation with Fe (III), Al (III) and Ga (III) and in Vivo Evaluation. *J. Inorg. Biochem.* **2002**, *92*, 43–54.

Table of Content Graphic

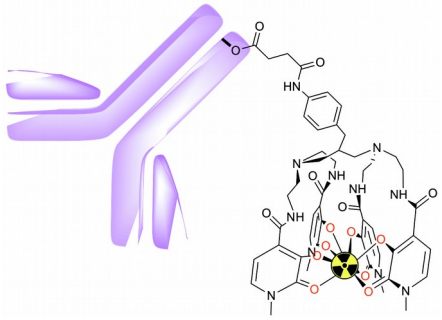

The solution state structure, thermodynamics, and spectroscopic properties of a new N-methyl-3,2-HOPO octadentate chelator developed for thorium-227 targeted alpha-therapy were comprehensively explored with a series of tri- and tetravalent metal cations. The chelator exhibits extreme thermodynamic selectivity towards tetravalent metal cations and excellent kinetics of bioconjugation with thorium as confirmed by one of the first examples of EXAFS characterization of a Th(IV) antibody conjugate.